arXiv:1105.0358v2 [nucl-th] 3 May 2011

Connecting scaling with short-range correlations

D. Berardo,[1] M. B. Barbaro,[2] R. Cenni,[3] T. W. Donnelly,[4] and A. Molinari[2]

[1]*Dipartimento di Fisica Teorica, Università di Torino, Via P. Giuria 1, 10125 Torino, Italy*

[2]*Dipartimento di Fisica Teorica, Università di Torino and INFN, Sezione di Torino, Via P. Giuria 1, 10125 Torino, Italy*

[3]*INFN, Sezione di Genova, Via Dodecaneso 33, I-16146 Genova, Italy*

[4]*Center for Theoretical Physics, Laboratory for Nuclear Science and Department of Physics, Massachusetts Institute of Technology, Cambridge, Massachusetts 02139, USA*

(Dated: January 20, 2013)

Abstract

We reexamine several issues related to the physics of scaling in electron scattering from nuclei. A basic model is presented in which an assumed form for the momentum distribution having both long- and short-range contributions is incorporated in the single-particle Green function. From this one can obtain saturation of nuclear matter for an NN interaction with medium-range attraction and short-range repulsion, and can obtain the density-density polarization propagator and hence the electromagnetic response and scaling function. For the latter, the shape of the scaling function and how it approaches scaling as a function of momentum transfer are both explored.

PACS numbers: 24.10.Cn; 25.30.-c

I. INTRODUCTION

Scaling phenomena as realized in electroweak interactions with nuclei at intermediate-to-high energies have several facets, including scaling of the first kind [1] (independence of the momentum transfer q) and second kind [2, 3] (independence of nuclear species, for instance, as characterized by the Fermi momentum k_F). In addition, universality for different reaction channels (longitudinal, transverse, *etc.*) has been called scaling of the zeroth kind [3, 4], while universality in the isoscalar and isovector channels has been called scaling of the third kind [5]. All four types of scaling are reasonably well respected by data at sufficiently high energies, namely away from threshold and for momentum transfers typically twice the Fermi momentum or larger, although there are observed to be scaling violations and their origins provide interesting insights into the dynamics of the scattering processes. For example, the transverse EM response is known to involve both the familiar one-body currents and two-body Meson-Exchange Currents (MEC) which do not scale in the same way [6–8, 10, 11].

In the present study we focus on one particular aspect of scaling, namely, scaling of the first kind. Our motivation is to explore the interconnections between the strong interaction dynamics of a representative NN potential that is chosen to provide the correct binding energy and saturation density of nuclear matter, on the one hand, and a corresponding Green function that is made to be consistent with those properties of nuclear matter, on the other. Having such a Green function one can immediately obtain the density-density polarization propagator and hence the longitudinal response R_L and scaling function F_L. For brevity these are called simply R and F in the rest of this work. In contrast to the usual approach, in the present study we "work backwards" assuming a form for the momentum distribution $n(k)$ and, given this, obtaining the corresponding energy per particle as a consequence. In particular, the chosen momentum distribution is taken to have both long-range contributions (those below and slightly above the Fermi surface) and short-range contributions which give rise to a tail that extends to high momentum.

To be able to carry out this study with much of the development still analytic we restrict our attention to the non-relativistic situation and assume a translationally invariant (infinite, homogeneous) many-body system of point nucleons. Our goal is not to provide a detailed numerical study of scaling phenomena for comparison with experiment, as this is better done with relativistic modeling, but is to provide insight into how the short-range part of the

momentum distribution which is important for obtaining saturation of nuclear matter also has a role to play in the corresponding scaling phenomena. We shall, however, explore several properties of scaling and scaling violations that are observed experimentally, namely, how scaling is approached for large momentum transfers q (in the scaling region it is approached from above, something most models fail to explain) and whether or not the present model is capable of explaining the observed asymmetry found in the scaling function.

In passing let us draw some comparisons with Deep Inelastic Scattering (DIS) of leptons on the proton which has been understood on the basis of the Bjorken scaling law and the parton model. There also one observes scaling violations which in the high-energy situation are coped with using the so-called evolution equations. Two basic assumptions lie at the foundations of Bjorken scaling (see, for example [9]): (1) the highly virtual photon interacts with the proton through point-like constituents (the partons) and (2) the partons cannot change their momenta during the extremely short time interval available for the DIS process and the parton-parton interactions are very weak, a situation referred to as asymptotic freedom. When taken into account the latter leads to scaling violations. In contrast, the situation of interest in the present work on electron scattering from strongly interacting nucleons in nuclei is apparently quite different. The model we use does not display the equivalent of asymptotic freedom and yet scaling is quite well obeyed, despite the strength of the partonic (nucleonic here) interactions. Of course our model will not be able to account for all types of scaling violations, namely those which stem from partonic sub-structures (gluons in QCD versus mesons in nuclei via meson exchange currents; the latter have been the subject in other studies, for instance, [7, 8]). In other words our nucleons (partons) are viewed as point-like. The very strong correlations between the nucleons induced by the short-range repulsion appear, at least in our model, to lend themselves to a description in terms of a mean field framework, in which the nucleons do not interact, apart from Pauli correlations. In other words the effect of the hard core is embedded in the modification of the nucleon momentum distribution with respect to that of the Fermi gas, still keeping an independent-particle model for the system. Thus to the extent that the mean field provides a realistic description of nuclei at large momenta, then scaling should occur, as we have found.

This paper, which is closely connected to the research developed in [12], outlines the model in Sect. II. Section III addresses the problems of linking the model to conventional

perturbation theory and focuses on the Coulomb Sum Rule (CSR), a quantity crucially dependent upon the pair correlation function (pcf) or, equivalently, upon the momentum distribution $n(k)$ of the nucleons in the nucleus. Indeed the CSR represents one of the best testing grounds for the pcf and $n(k)$. In Sect. IV the fermion propagator, the key element in constructing the response of our system to an external probe and hence the scaling function, is set up. All the issues connected with scaling and the results we have obtained with our approach are collected in Sect. V, and then finally in Sect. VI we summarize our main conclusions from this study.

II. THE MODEL

The basic formula we start with reads [13] (we use $\hbar = c = 1$)

$$\frac{E}{A} = \frac{4V}{A} \int \frac{d\vec{k}}{(2\pi)^3} \frac{k^2}{2m} n(k) + \frac{1}{2A} \int d\vec{r}_1 d\vec{r}_2 v(\vec{r}_1 - \vec{r}_2) C(\vec{r}_1 - \vec{r}_2) \ , \tag{1}$$

where the factor of 4 accounts for the spin-isospin degeneracy (a summation over these variables is of course understood in the second term as well) and A is the particle number. Equation (1) yields the ground-state energy of the system (actually the energy per particle). We apply it to an infinite, homogeneous, non-relativistic ensemble of nucleons, viewed as enclosed in a large volume V to be let to go to infinity at the end of the calculation. We assume that a two-body force acts between the nucleons and that this is described by the potential $v(r)$, where $r = |\vec{r}_1 - \vec{r}_2|$. In Eq. (1) $C(\vec{r}_1 - \vec{r}_2)$ is the pcf simply related by a Fourier transform to the $n(k)$ in our spatially homogeneous system.

Now, rather than attempting to compute $n(k)$ starting from the potential $v(r)$ adopting one of the various many-body techniques available for the purpose (for example a perturbative one), we *assume* the momentum distribution to be parametrized as

$$n(k) = \theta(k_F - k)\Big(1 - \alpha \frac{k^2}{k_F^2}\Big) + \theta(k - k_F)\beta_1 e^{-\beta_2(\frac{k}{k_F} - 1)}, \tag{2}$$

accounting both for the existence of a high-momentum tail in $n(k)$, as suggested by the presently available experimental information, as well as standard theory (see, for example, a recent treatment of the momentum distribution and spectral function in [14]), and for the Luttinger theorem which guarantees the existence of a Fermi surface for a "normal"

interacting Fermi system. Of course $n(k)$ (Eq. 2) should fulfill the constraint

$$\begin{aligned}\frac{A}{V} &= 4\int\frac{d\vec{k}}{(2\pi)^3}n(k) = \frac{2}{\pi^2}\Big\{\int_0^{k_F}k^2dk\Big(1-\alpha\frac{k^2}{k_F^2}\Big)+\beta_1\int_{k_F}^{\infty}k^2dke^{-\beta_2(\frac{k}{k_F}-1)}\Big\}\\ &= \frac{2k_F^3}{3\pi^2}\Big(1-\alpha\frac{3}{5}+3\frac{\beta_1}{\beta_2^3}(\beta_2^2+2\beta_2+2)\Big) = \frac{2k_F^3}{3\pi^2}h(\alpha,\beta_1,\beta_2) = n_0, \qquad (3)\end{aligned}$$

n_0 being the system's constant density.

¿From Eq. (2) the pcf is obtained according to the definition

$$\begin{aligned}C(\vec{r}_1-\vec{r}_2) &= \sum_{\gamma,\delta}<\Psi_0|\hat{\Psi}_\gamma^\dagger(\vec{r}_1)\hat{\Psi}_\delta^\dagger(\vec{r}_2)\hat{\Psi}_\delta(\vec{r}_2)\hat{\Psi}_\gamma(\vec{r}_1)|\Psi_0>\\ &= \Big(\frac{A}{V}\Big)^2-4\Big[h(\alpha,\beta_1,\beta_2)\int\frac{d\vec{k}}{(2\pi)^3}e^{-i\vec{k}\cdot\vec{r}}n(k)\Big]^2 = n_0^2\Big\{1-\frac{1}{4}g^2(r)\Big\} \qquad (4)\end{aligned}$$

and one gets

$$\begin{aligned}C(r) &= n_0^2\Big\{1-\frac{1}{4}\Big\{\frac{3}{k_Fr}\Big[j_1(k_Fr)-\frac{\alpha}{(k_Fr)^4}\Big(3((k_Fr)^2-2)\sin(k_Fr)-\\ &-k_Fr((k_Fr)^2-6)\cos(k_Fr)\Big)+\beta_1\Big(\frac{k_Fr}{(k_Fr)^2+\beta_2^2}\Big)^2\times \qquad (5)\\ &\times\Big(\sin(k_Fr)\Big(\beta_2+\frac{\beta_2^2+\beta_2^3}{(k_Fr)^2}-1\Big)+\cos(k_Fr)\Big(k_Fr+\frac{2\beta_2+\beta_2^2}{k_Fr}\Big)\Big)\Big]\Big\}^2\Big\}\ .\end{aligned}$$

In Eq. (4) $|\Psi_0>$ is the system's ground state and $\hat{\Psi}_\gamma(\vec{r}_1)$ and $\hat{\Psi}_\delta(\vec{r}_2)$ are the fermion fields. Furthermore the above formula holds valid for infinite nuclear matter. If we need the pcf only for protons, as in the case of the CSR, then the factor $\frac{1}{4}$ should clearly be replaced with a factor $\frac{1}{2}$ in front of the second term on the right-hand side of Eq. (5) and one should set $n_0 = Z/V$, Z being the number of protons. As seen in the above equations the pcf naturally splits into a direct and an exchange contribution (the first and the second terms on the right-hand side of Eq. (4)).

In passing we note that by setting $\alpha = \beta_1 = \beta_2 = 0$ in Eq. (5), namely by recovering the theta-function momentum distribution of a non-interacting Fermi system, we get back the well-known pcf of a Fermi gas

$$C(r) = n_0^2\Big[1-\frac{1}{4}\Big(\frac{3j_1(k_Fr)}{k_Fr}\Big)^2\Big] \qquad (6)$$

which identifies $g(r)$ with $\frac{3j_1(k_Fr)}{k_Fr}$.

Now by inserting Eqs. (2) and (5) into Eq. (1) we obtain the binding energy per particle of the nuclear system providing the potential $v(r)$ is known. For the latter we employ a

schematic model which retains only the basic features of the nucleon-nucleon force since, as already emphasized, our aim is not a precise reproduction of the experimental data. Accordingly we employ a mixture of a Wigner and a Majorana force, namely

$$v(r) = u(r)[1 - \gamma + \gamma P_x] = \begin{cases} +U_0 \;\; \gamma = 0 & r \leq a \\ -V_0 \;\; \gamma = \frac{1}{2} & a \leq r \leq b \\ 0 & b \leq r, \end{cases} , \tag{7}$$

where P_x is the space exchange operator and γ a parameter varying in the range $0 \leq \gamma \leq 1$. In accord with common wisdom we choose for γ the values indicated in Eq. (7) where one recognizes the strong short-range repulsion and the moderate intermediate-range attraction characterizing the nucleon-nucleon interaction.

Now all of the elements to compute the behaviour of the E/A versus k_F are available. We get

$$\begin{aligned} \frac{E}{A} = \frac{4}{n_0}\frac{4\pi}{(2\pi)^3}\frac{1}{2m}\int_0^\infty dk k^4 n(k) \;+\; & \frac{n_0}{2}4\pi\int_0^\infty dr r^2\Big[U_0\theta(a-r) - \frac{3}{8}V_0\theta(b-r)\theta(r-a)\Big] \\ - \; & \frac{n_0}{2}4\pi\frac{1}{4}\int_0^\infty dr r^2\Big[U_0\theta(a-r) + \frac{3}{2}V_0\theta(b-r)\theta(r-a)\Big]g^2(r) \; . \end{aligned} \tag{8}$$

The numerical factors appearing in the potential terms stem from summing over the spin-isospin variables of the interacting nucleons; they of course enter differently in the direct and exchange contributions to E/A, namely the second and the third terms on the right-hand side of Eq. (8).

Before actually displaying the behaviour of E/A versus k_F we have to face the crucial problem of fixing the values of the seven parameters (four for the potential $v(r)$, three for the momentum distribution $n(k)$) needed to render our approach predictive. In order to tackle this problem we proceed as follows: we start by choosing "reasonable" values. Next we compute Eq. (8) using these chosen values and repeat the procedure adjusting at each step the parameters until they yield $E/A \sim$ -16 MeV and, for the compression modulus, $\kappa = \frac{k_F^2}{9}\frac{\partial^2 E/A}{\partial k_F^2} \sim 14$ MeV [15] at the minimum of the curve, that should occur at a value of k_F which, when inserted into Eq. (3), provides the experimental density of nuclear matter, namely 0.17 fm^{-3}.

The three above mentioned constrains (energy, density and compressibility) turn out to be fulfilled by choosing

$$\alpha = 0.2, \quad \beta_1 = 0.4, \quad \beta_2 = 4 \tag{9}$$

and

$$U_0 = 2.5 \text{ GeV}, \quad V_0 = 53 \text{ MeV}, \quad a = 0.465 \text{ fm}, \quad b = 2.10 \text{ fm} . \tag{10}$$

With these values the minimum of the curve yielding E/A versus k_F occurs at k_F=1.23 fm^{-1}, which is obviously different from the value of the pure Fermi gas, namely k_F=1.36 fm^{-1} .

The associated E/A versus k_F is displayed in Fig. 1 which yields

$$\left(\frac{E}{A}\right)_{\text{min}} = -15.68 \text{ MeV}, \quad (k_F)_{\text{min}} = 1.23 \text{ fm}^{-1}, \quad (\kappa)_{\text{min}} = 13.8 \text{ MeV} , \tag{11}$$

namely the experimental values.

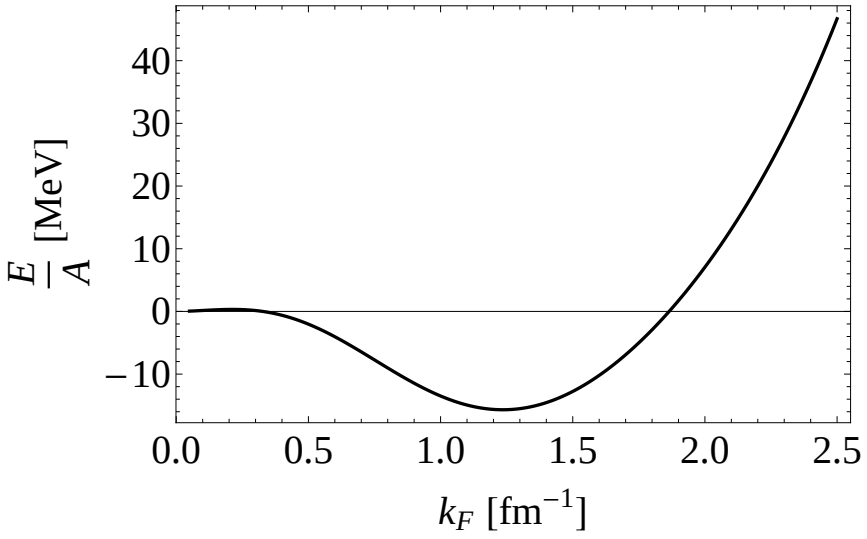

FIG. 1: The binding energy (E/A) versus k_F, as given by Eq. (8).

We also display the momentum distribution $n(k)$ in Fig. 2. Concerning the results of this section, it should be clear that the choice of the parameters given in Eq. (10) is far from unique, and that these values should be viewed as providing a first orientation on a complex problem. Our goal is only to use something representative for the potential in attempting to shed light on the connections between saturation of nuclear matter and electron scattering scaling phenomena.

III. THE MANY-BODY CONTENT OF $n(k)$ AND THE CSR

Next the question arises: which are the Feynman diagrams one has to take into account in order to obtain the $n(k)$ given by Eq. (2)? This is equivalent to asking: what kind of

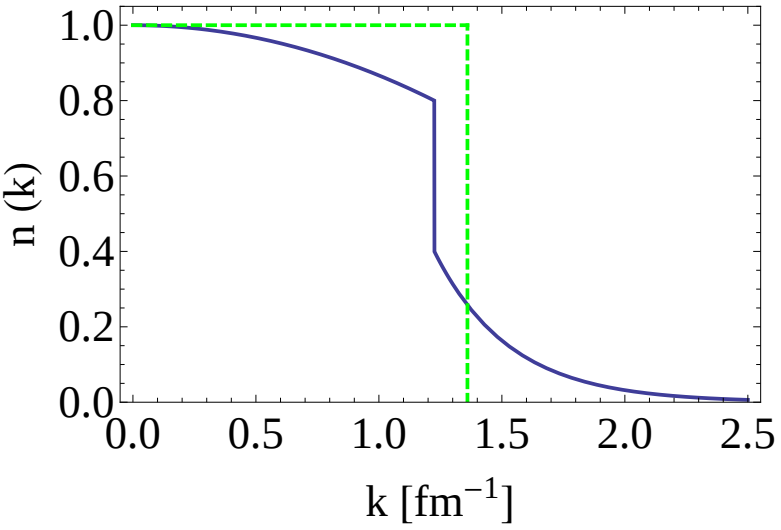

FIG. 2: (color online) Solid (blue online): the momentum distribution $n(k)$ versus k. Also displayed (dashed, green online) is the Fermi gas $n(k) = \theta(k_F - k)$ with $k_F = 1.36$ fm^{-1}.

correlations among nucleons are responsible for changing the theta-function into our $n(k)$ which we assumed to be the true momentum distribution of our system?

To help in better grasping the relevance of this question it is of importance to realize that if we replace in Eq. (1) $n(k)$ with $\theta(k_F - k)$ and $C(\vec{r}_1 - \vec{r}_2)$ with Eq. (6) we obtain

$$\begin{aligned}\frac{E}{A} \;=\; & \frac{3}{5}\frac{k_F^2}{2m} + n_0\Big[\frac{2}{3}\pi a^3 U_0 - \frac{\pi}{4}(b^3 - a^3)V_0\Big] \\ & -\frac{1}{\pi}\Big(U_0 - \frac{3}{2}V_0\Big)\Big[\mathrm{Si}(2k_F a) + \frac{\cos(2k_F a) - 3}{2k_F a} + \frac{\cos(2k_F a) - 1}{2(k_F a)^3} + \frac{\sin(2k_F a)}{(k_F a)^2}\Big] \\ & -\frac{3}{2\pi}V_0\Big[\mathrm{Si}(2k_F b) + \frac{\cos(2k_F b) - 3}{2k_F b} + \frac{\cos(2k_F b) - 1}{2(k_F b)^3} + \frac{\sin(2k_F b)}{(k_F b)^2}\Big]\,, \end{aligned} \tag{12}$$

namely the result provided by Hartree-Fock (HF) theory [15], which, as is well known, captures the content of the two first-order perturbative diagrams shown in Fig. 3. It is instructive to look at the result one gets in HF with the parameters given in Eq. (10) for the double square well potential of Eq. (7). This is displayed in Fig. 4: here we see that E/A in HF still saturates, although at a far too low density ($k_F = 1.02$ fm^{-1}) and with a far too low energy ($E/A = -1.56$ MeV).

To prove that by summing all perturbative diagrams one would recover the $n(k)$ of Eq. (2) (and hence the E/A of Fig. 1) is clearly an impossibility. In the present study our approach is only to explore a simple model while attempting to maintain as high a level of coherence as we can. To achieve the latter we first resort to Calogero's theorem [16], which states that

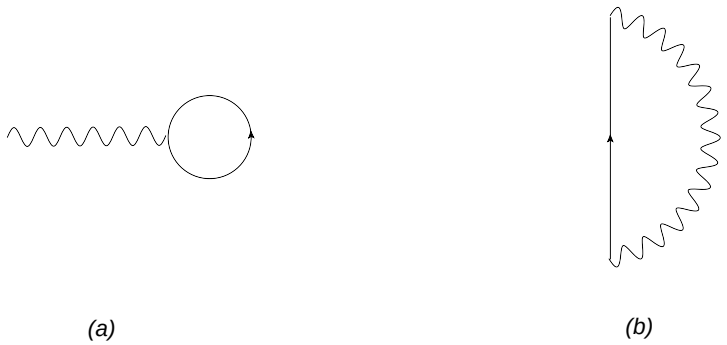

FIG. 3: First-order proper self-energy $\Sigma^{\star}_{(1)}$; in (a) and (b) are shown the direct and exchange terms, respectively.

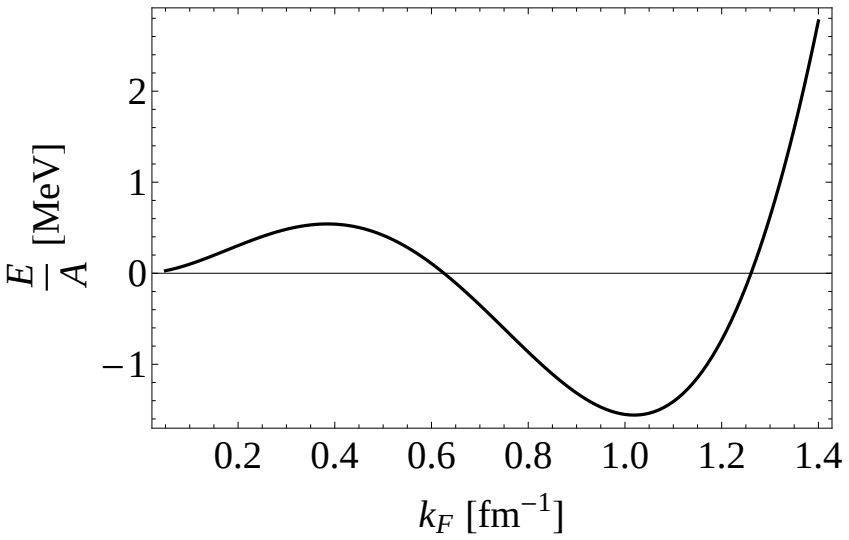

FIG. 4: E/A versus k_F in HF theory employing the potential of Eq. (7) with the parameters of Eq. (10).

for a homogeneous infinite system asympotically one should have

$$n(k) \sim \left[2mn_0 \frac{\tilde{v}(k)}{k^2}\right]^2, \tag{13}$$

where, in the present case,

$$\tilde{v}(k) = \int d\vec{r} e^{-i\vec{k}\cdot\vec{r}} v(r) = \frac{4}{3}\pi a^3 \left\{ U_0 \frac{3j_1(ka)}{ka} - V_0 \left[\frac{b^3}{a^3} \frac{3j_1(kb)}{kb} - \frac{3j_1(ka)}{ka} \right] \right\} . \tag{14}$$

In Fig. 5 we compare our $n(k)$ with the Calogero's theorem predictions: we do so in the range of momenta starting from the Fermi surface ($k = k_F = 1.23$ fm^{-1}) up to $k \sim 3.6$ fm^{-1},

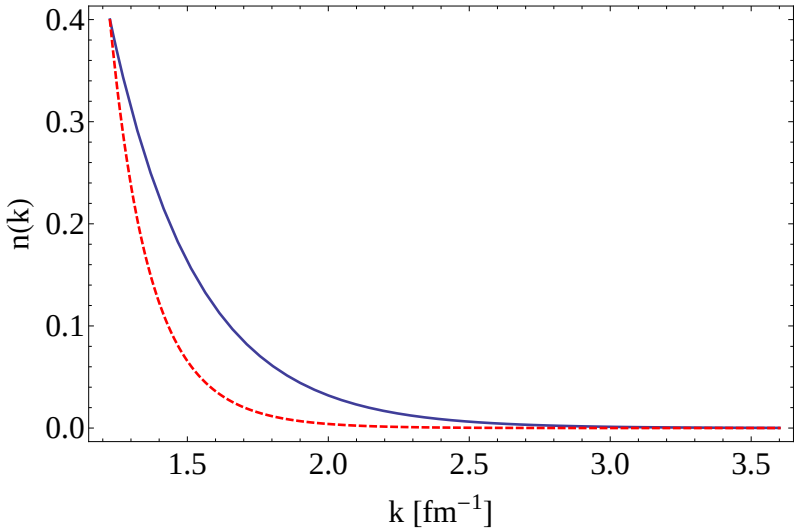

FIG. 5: (color online) Solid line (blue online): the momentum distribution of Eq. (2). Dashed line (red online): Calogero asymptotic behaviour Eq. (13), multiplied by a factor 2×10^{-4} (see text for the origin of this factor).

since for larger momenta both distributions become so small that they render the comparison meaningless. In Fig. 5 one sees that the two curves are not too different; hence our $n(k)$ and $\widetilde{v}(r)$, while not exactly the same, nevertheless display an acceptable degree of coherence. It should be stated that in carrying out such a comparison, unfortunately, Calogero's theorem does not quantify the value of q signalling the onset of the asymptotic regime, and hence we have arbitrarily normalized the Calogero's asymptotic momentum distribution in such a way to have it coincide with our $n(k)$ at the Fermi surface.

Concerning the question related to the measurement of $n(k)$, we recall that access to information on this is offered by the CSR, which in fact essentially depends "only" upon the momentum distribution at least within the context of the present model. Indeed from unitarity one has

$$S(q) = Z - n_0^2 V \frac{1}{2} \int d\vec{r} e^{-i\vec{q}\cdot\vec{r}} g^2(r), \tag{15}$$

where $g(r)$ (see Eq. (5)) is directly fixed by the Fourier transform of our $n(k)$.

For sake of completness we display in Fig. 6 the CSR predicted by our $n(k)$. Actually this curve was already shown in [12], however we revisit it once more here to illustrate how the attainement of the asymptotic value (namely one) is postponed by the nucleon-nucleon correlations, in particular, the repulsive short-range ones, to larger values of q ($\cong 4.6$ fm^{-1})

than for the Fermi gas situation ($\cong 2.46$ fm^{-1}).

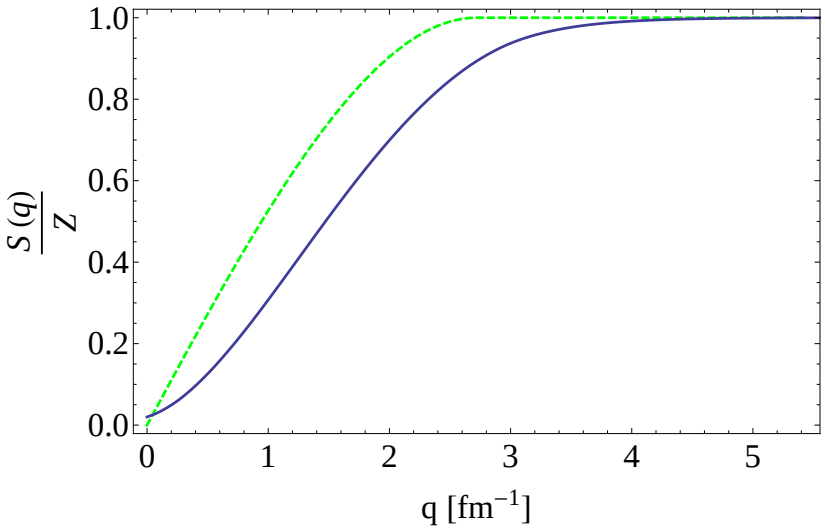

FIG. 6: (color online) The CSR for a free Fermi gas (dashed line, green online) and for a correlated one according to our model (solid line, blue online).

To illustrate our second path toward coherence we commence by recalling the alternative model of [17], which deals with the same issues treated in the present paper, namely the scaling function and momentum distribution, but with a different philosophy. The study of [17] is based on the use of PWIA (Plane-Wave Impulse Approximation) and has as its starting point the assumption of the factorization of the one-particle exclusive cross section (namely the cross section for the process $(e, e'N)$) according to the expression

$$\left[\frac{d\sigma}{d\epsilon' d\Omega' dp_N d\Omega_N}\right]^{\rm PWIA} = K\sigma^{eN}(q,\omega;p,\mathcal{E},\phi_N)S(p,\mathcal{E})\ . \tag{16}$$

In the above K is a kinematical factor, σ^{eN} the eN single-nucleon cross section and $S(p,\mathcal{E})$ the nucleon spectral function expressed in terms of the so-called missing-energy and missing-momentum variables (for their definition see, for instance, [19]). We do not dwell here on the procedure leading from Eq. (16) to the scaling function: this topic has been addressed a number of times in the literature. Suffice it to say that the key step is the integration of Eq. (16) over the variables p and $\mathcal{E}$ in a domain which has been analyzed in the past and whose boundaries are set by energy and momentum conservation. The above procedure corresponds to passing from the semi-inclusive $(e, e'N)$ cross section to the inclusive (e, e') cross section. Indeed one has

$$\frac{d\sigma}{d\epsilon' d\Omega'} = \overline{\sigma}^{eN}(q,\omega;p=|y|,\mathcal{E}=0)F(q,\omega), \tag{17}$$

where $\overline{\sigma}^{eN}$ is evaluated at the minimum values of $\mathcal{E}$ and p allowed by kinematics. The scaling function $F(q,\omega)$ is easily found to read

$$F(q,\omega) = 2\pi \int\int_{\Sigma(q,\omega)} pdpd\mathcal{E}S(p,\mathcal{E}) \tag{18}$$

in PWIA. Now if the integration domain $\Sigma(q,\omega)$ in Eq. (18) extends up to encompass the limiting value $\mathcal{E} \to \infty$ then the scaling function can be linked to the momentum distribution according to [24]

$$n(p) = \int_0^\infty d\mathcal{E}\, S(p,\mathcal{E})\,. \tag{19}$$

Thus, at variance with our method which is based on the coherence between the momentum distribution and the scaling function, in the sense of having both of them derived within the same theory, in [17] the strategy is to exploit the link between the scaling function and the momentum distribution and hence the possibility of extracting information on $n(k)$ from (e,e') experimental data.

IV. SETTING UP THE SINGLE-NUCLEON PROPAGATOR

Our scheme is based on the central role played by the single-fermion propagator $G(\vec{k},\omega)$ for nucleons in the nucleus. In fact, as is well known, knowledge of the latter gives access to the E/A according to the expression [18]

$$E = \frac{iV}{2(2\pi)^4} \lim_{\eta\to 0^+} \int d\vec{k} \int_{-\infty}^{\infty} d\omega e^{i\omega\eta} \Big(\frac{k^2}{2m} + \omega\Big) \mathrm{Tr} G(\vec{k},\omega) \tag{20}$$

and to the scaling function according to the formula

$$F(q,\omega) = -\frac{q}{m}\frac{V}{\pi} \mathrm{Im}\Pi(q,\omega)\ . \tag{21}$$

This represents the content of linear response theory and, as in [17], assumes the factorization of the single-nucleon cross section. In Eq. (21) $\Pi(q,\omega)$ is referred to as the polarization propagator or, in coordinate space, as the density-density correlation function. In field theory language it corresponds to a particular choice of the field arguments in the two-particle propagator and in momentum space reads

$$\Pi(q,\omega) = -\frac{i}{2}\int \frac{d^4k}{(2\pi)^4} G(k+q)G(k). \tag{22}$$

Knowing G ensures control of $\Pi(q,\omega)$ and this, in turn, through Eq. (21), permits the determination of the scaling function $F(q,\omega)$. Also, in a coherent scheme, $G(k)$ should yield the correct momentum distribution (namely our $n(k)$).

Can such a propagator be derived on the basis of the knowledge of $n(k)$ alone? The answer is yes in the simple approach taken in the present work where an infinite, homogeneous many-body system of nucleons has been assumed. This kind of mean-field approximation possesses a remarkably coherent structure; whether this remains true in a more sophisticated many-body framework has yet to be proven. Continuing to work within the context of our simple model, as a first step to achieve this goal we rewrite our basic expression in Eq. (1), exploiting the Faltung theorem of Fourier analysis. For this purpose, we start from

$$\begin{aligned}\frac{E}{A} &= \frac{4V}{A}\int\frac{d\vec{k}}{(2\pi)^3}\frac{k^2}{2m}n(k)+\frac{n_0}{2}\int d\vec{r}v(r)\Big(1-\frac{1}{4}g^2(r)\Big)\\ &= \frac{4}{n_0}\int\frac{d\vec{k}}{(2\pi)^3}\frac{k^2}{2m}n(k)+\frac{n_0}{2}\Big[\int d\vec{r}v_D(r)-\frac{1}{4}\int d\vec{r}v_E(r)g^2(r)\Big]\end{aligned} \tag{23}$$

with $g^2(r)$ given by Eq. (4) and the direct and the exchange potential terms by Eq. (8) in coordinate space and introducing the Fourier representations according to

$$\tilde{v}_D(k)=\int d\vec{r}e^{-i\vec{k}\cdot\vec{r}}v_D(r)=\frac{4\pi}{3}U_0a^3\frac{3j_1(ka)}{ka}-\frac{\pi}{2}V_0\Big(b^3\frac{3j_1(kb)}{kb}-a^3\frac{3j_1(ka)}{ka}\Big)\,, \tag{24}$$

$$\tilde{v}_E(k)=\int d\vec{r}e^{-i\vec{k}\cdot\vec{r}}v_E(r)=\frac{4\pi}{3}\Big[a^3\frac{3j_1(ka)}{ka}\Big(U_0-\frac{3}{2}V_0\Big)+\frac{3}{2}V_0b^3\frac{3j_1(kb)}{kb}\Big] \tag{25}$$

and

$$\int d\vec{r}e^{-i\vec{k}\cdot\vec{r}}\Big(1-\frac{1}{4}g^2(r)\Big)=(2\pi)^3\delta(\vec{k})-\frac{4}{n_0^2}h^2(\alpha,\beta_1,\beta_2)\int\frac{d\vec{p}}{(2\pi)^3}n(p)n(|\vec{k}-\vec{p}|). \tag{26}$$

Then, with the help of Eqs. (24–26), we obtain

$$\frac{E}{A}=\frac{4}{n_0}\int\frac{d\vec{k}}{(2\pi)^3}n(k)\Big[\frac{k^2}{2m}+\frac{n_0}{2}\tilde{v}_D(0)-\frac{h^2(\alpha,\beta_1,\beta_2)}{2}\int\frac{d\vec{q}}{(2\pi)^3}n(q)\tilde{v}_E(|\vec{k}+\vec{q}|)\Big]=\frac{4}{n_0}\int\frac{d\vec{k}}{(2\pi)^3}\epsilon_k^{(h)}, \tag{27}$$

where

$$\epsilon_k^{(h)}=n(k)\Big[\frac{k^2}{2m}+\frac{n_0}{2}\tilde{v}_D(0)-\frac{h^2(\alpha,\beta_1,\beta_2)}{2(2\pi)^2}\int_0^\infty dpp^2\tilde{v}_E(p)\int_{-1}^1 dxn(|\vec{p}-\vec{k}|)\Big] \tag{28}$$

is the single-hole energy displayed in Fig. 7. For comparison, in Fig. 8 the single-particle energy

$$\epsilon_k^{(p)}=\frac{1-n(k)}{n(k)}\epsilon_k^{(h)} \tag{29}$$

is shown. Note the discontinuity of ~ 6.5 MeV in both $\epsilon_k^{(h)}$ and $\epsilon_k^{(p)}$ at the Fermi surface, the vanishing at large k of $\epsilon_k^{(h)}$ and the value

$$\begin{aligned}
\epsilon_0^{(h)} &= \frac{n_0}{2}\tilde{v}_D(0) - \frac{h^2(\alpha,\beta_1,\beta_2)}{(2\pi)^2}\int_0^\infty dpp^2\tilde{v}_E(p)n(p) \\
&= \frac{n_0}{2}\frac{4\pi}{3}a^3\Big[U_0 - \frac{3}{8}V_0\Big(\frac{b^3}{a^3}-1\Big)\Big] \\
&\quad -\frac{h^2(\alpha,\beta_1,\beta_2)}{\pi}\Big\{\Big(U_0-\frac{3}{2}V_0\Big)\Big[\mathrm{Si}(k_Fa)-(1-\alpha)\sin(k_Fa)-3\alpha j_1(k_Fa)\Big] \\
&\qquad +\frac{3}{2}V_0\Big[\mathrm{Si}(k_Fb)-(1-\alpha)\sin(k_Fb)-3\alpha j_1(k_Fb)\Big] \\
&\quad +\beta_1\Big(U_0-\frac{3}{2}V_0\Big)\Big[k_Fa\frac{k_Fa\sin(k_Fa)-\beta_2\cos(k_Fa)}{(k_Fa)^2+\beta_2^2}+e^{\beta_2}\mathrm{ImE}_1(\beta_2-ik_Fa)\Big] \\
&\qquad +\beta_1\frac{3}{2}V_0\Big[k_Fb\frac{k_Fb\sin(k_Fb)-\beta_2\cos(k_Fb)}{(k_Fb)^2+\beta_2^2}+e^{\beta_2}\mathrm{ImE}_1(\beta_2-ik_Fb)\Big]\Big\} \\
&= -77.90 \text{ MeV}
\end{aligned} \tag{30}$$

of the latter at the origin.

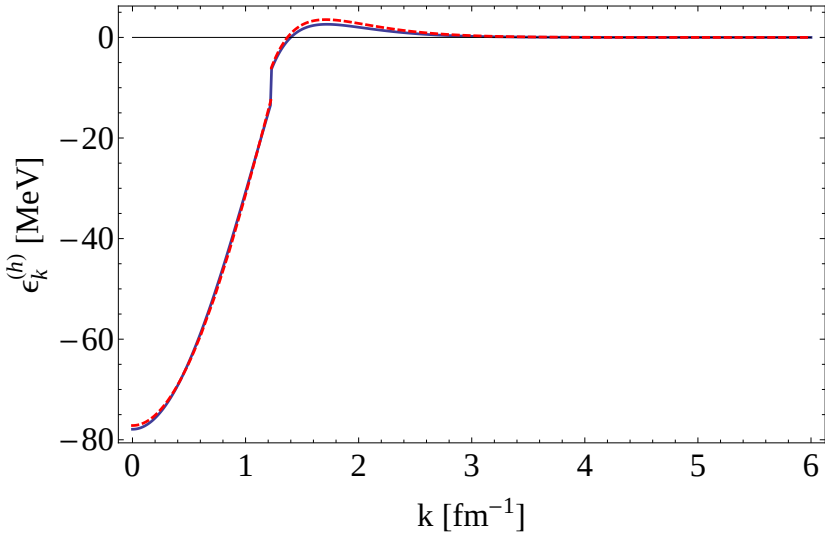

FIG. 7: (color online) Single-particle energy (hole) of our model shown for $k_F = 1.23$ fm^{-1} which corresponds to the saturation density of the system. The dashed line represents the fit given by Eq. (32).

The above single-particle energies yield the poles of the fermion propagator which, as a consequence, can then be cast into the form

$$G(k,\omega) = \frac{n(k)}{\omega - n(k)[\frac{k^2}{2m}+\frac{n_0}{2}\tilde{v}_D(0)-\frac{h^2(\alpha,\beta_1,\beta_2)}{2(2\pi)^2}\int_0^\infty dpp^2\tilde{v}_E(p)\int_{-1}^1 dxn(|\vec{p}-\vec{k}|)]-i\eta} \tag{31}$$

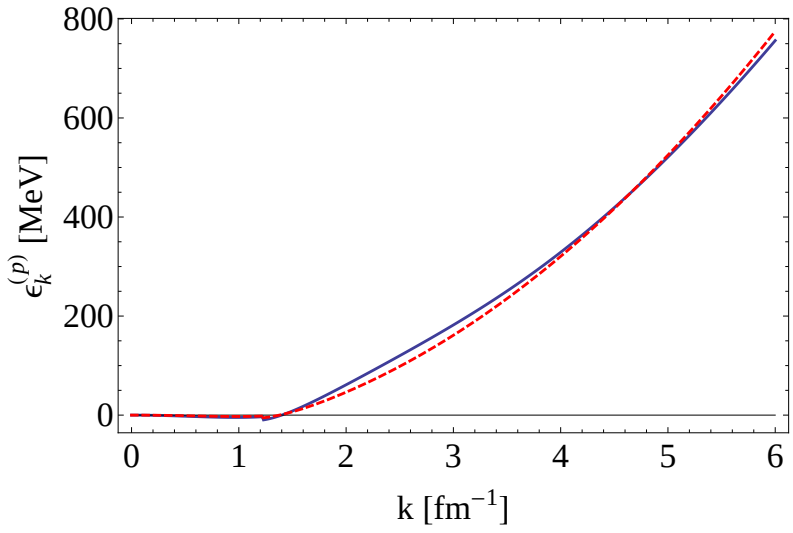

FIG. 8: (color online) Single-particle energy (particle) of our model shown for $k_F = 1.23$ fm^{-1} which corresponds to the saturation density of the system. The dashed line represents the fit given by Eq. (33).

$$+\frac{1-n(k)}{\omega-[1-n(k)][\frac{k^2}{2m}+\frac{n_0}{2}\tilde{v}_D(0)-\frac{h^2(\alpha,\beta_1,\beta_2)}{2(2\pi)^2}\int_0^\infty dpp^2\tilde{v}_E(p)\int_{-1}^1 dxn(|\vec{p}-\vec{k}|)]+i\eta}\ .$$

This structure of the propagator tells us that in our model the holes exist below, but also above, the Fermi surface. Likewise the particles exist above, but also below, the Fermi surface. These occurrences clearly reflect the behaviour of our momentum distribution. The important point to be stressed, however, is that the propagator in Eq. (31) provides the correct system energy and $n(k)$.

Now, to pave the way to the actual evaluation of Π, it helps to realize that, although the expression of the single-particle energies is far from being simple (in fact it cannot be expressed analytically), nevertheless its k dependence lends itself to be suitably represented, apart from the factor $n(k)$, by a parabola. This is reminiscent of HF theory. Hence we use the following quite faithful representation

$$\epsilon^{(h)}(k) = n(k)(A_{(h)} + B_{(h)}k^2) = n(k)\Big(A_{(h)} + \frac{k^2}{2m^\star_{(h)}}\Big) \tag{32}$$

with $A_{(h)} = -77.16$ MeV and $B_{(h)} = 41.10$ MeV fm^2, yielding an effective mass $m^\star_{(h)} = 0.50$ m for holes and

$$\epsilon^{(p)}(k) = (1-n(k))(A_{(p)} + B_{(p)}k^2) = (1-n(k))\Big(A_{(p)} + \frac{k^2}{2m^\star_{(p)}}\Big) \tag{33}$$

with $A_{(p)} = -43.09$ MeV and $B_{(p)} = 22.72$ MeV fm^2, yielding an effective mass $m^\star_{(p)} = 0.91$ m for particles. It is indeed startling to realize how large the impact of our two-body interaction in Eq. (7) is on the effective hole mass, the generally accepted ratio being actually $m^*/m \simeq 0.83$ [20]. How faithful Eq. (32) and Eq. (33) are in providing the single-particle energies, can be garnered from Figs. 7 and 8.

Finally, the response function of the system is easily derived,

$$R(q,\omega) = -\frac{V}{\pi}\mathrm{Im}\Pi(q,\omega), \tag{34}$$

and from the response one immediately obtains the scaling function per proton according to

$$\begin{aligned} F(q,\omega) &= \frac{q}{m}\frac{R(q,\omega)}{Z} \\ &= \frac{q}{m}\frac{1}{n_0}\frac{1}{\pi^2}\int_0^\infty dk k^2 n(k)\int_{-1}^1 dx[1-n(|\vec{k}+\vec{q}|)]\delta[\omega-\epsilon^{(p)}(|\vec{k}+\vec{q}|)+\epsilon^{(h)}(k)], \end{aligned} \tag{35}$$

where the trivial frequency and azimuthal integrations have been performed. The results of our numerical calculations of Eq. (35) are reported in the next section. Following standard practice when discussing scaling we shall show results for the dimensionless scaling function

$$f(q,\omega) \equiv k_F \times F(q,\omega) \tag{36}$$

which takes on an especially simple form for the relativistic Fermi gas (see, *e.g.,* [2, 3]).

V. RESULTS

In Figs. 9 and 10 the results for the response $R(q,\omega)$ (Eq. (34)) and scaling function $f(q,\omega)$ (Eq. (36)) are shown versus ω for a range of momentum transfers. The response and the scaling function for the free Fermi gas are also displayed for comparison.

We observe the following:

- The response and scaling function obtained using our model, as expected, span a range of energy loss that extends to larger values than that seen for the Fermi gas model — a clear indication of the role of correlations among the nucleons. The widths seen in our model are somewhat larger than those of the Fermi gas and the peak heights are somewhat lower, both in better accord with experimental data.

- The peak positions in our model are shifted to higher energy loss than for the Fermi gas (see also the discussions to follow).

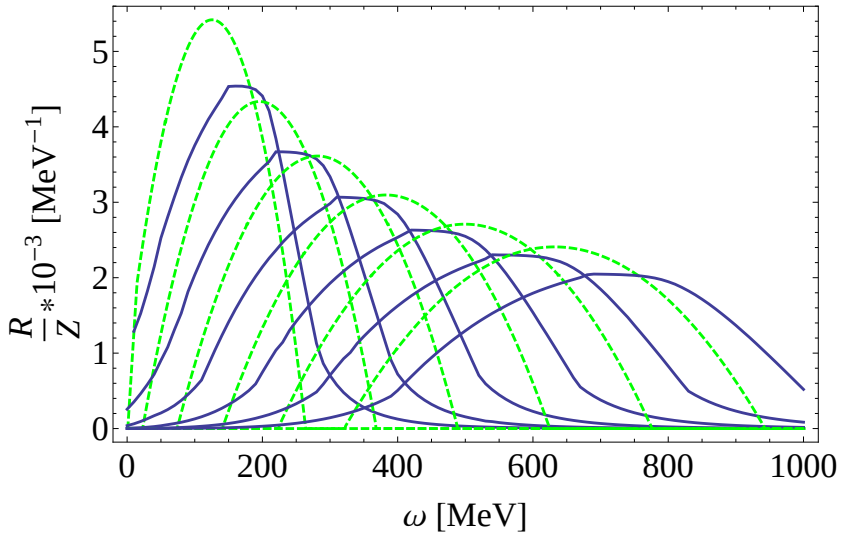

FIG. 9: (color online) The response function of our model (solid line, blue online) and the response function of a free Fermi gas (dashed line, green online) plotted versus ω for $q = 2k_F = 2.46$ fm^{-1} up to $q = 4.5k_F = 5.53$ fm^{-1} in steps of $0.5k_F$. Results for lower values of q peak at lower values of ω.

- Unlike for the Fermi gas model our $R(q,\omega)$ and $f(q,\omega)$ are no longer perfectly symmetric around their maxima. While approximately so, they have tails that extend both to higher and lower values of ω. However, the degree of asymmetry is not as large as what is observed experimentally.

- Note that while the height of $R(q,\omega)$ decreases with q, the height of $f(q,\omega)$ remains constant.

To investigate the scaling behaviour of our results we follow the usual procedures and display f, not versus ω as above, but versus the well-known non-relativistic scaling variable [21]

$$\psi_{nr} = \frac{1}{k_F}\left(\frac{m\omega}{q} - \frac{q}{2}\right). \tag{37}$$

Now we indeed see in Fig. 11 that the scaling functions for different values of q tend to group together very closely when displayed versus ψ_{nr}, that is they scale. Noting that the coalescence in our model occurs at a peak value other than $\psi_{nr} = 0$, it is interesting to investigate whether a simple modification of the scaling variable different from the one of Eq. (37) can be devised to shift the peak position to zero. One can always do this by

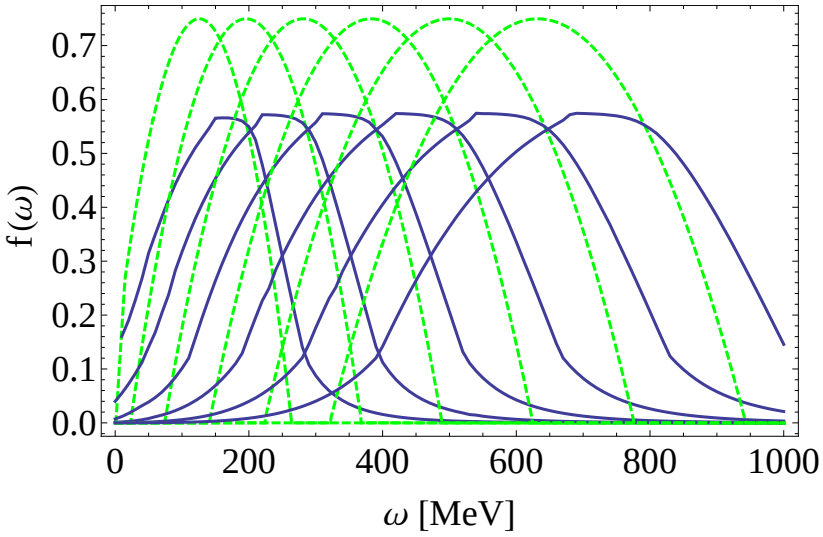

FIG. 10: (color online) The scaling function of our model (solid line, blue online) and the scaling function of a free Fermi gas (dashed line, green online) plotted versus ω for the same values of q used in Fig. 9.

employing the variable

$$\psi'_{nr} \equiv \frac{1}{k_F}\left(\frac{m\omega'}{q} - \frac{q}{2}\right), \tag{38}$$

where $\omega' = \omega - E_{shift}(q)$, and where $E_{shift}(q)$ is a q-dependent energy shift. If one uses the simple parametrization

$$E_{shift}(q) = E_0 + E_1(q/k_F) \tag{39}$$

with $E_0 = -17.4$ MeV and $E_1 = 15.9$ MeV (see Fig. 13), then almost perfect scaling centered about $\psi'_{nr} = 0$ is attained, as seen in Fig. 12. It appears that the impact of the NN interactions that have been incorporated in the present model is felt via a q-dependent shift in the definition of this new scaling variable, although a direct connection to the underlying dynamics is not obvious. As is clear from Fig. 13 similar shifting is seen using relativistic mean field theory. One of course should not expect these to be identical, since the present model is non-relativistic while the RMF results are obtained using a relativistic model. In either case, while the shift is qualitatively what is observed experimentally, it is probably somewhat too strong in both cases [22, 23].

In Fig. 14 we show the same results as in Fig. 12, but now on a semilog scale. The asymmetry, while small, is clearly apparent. More strength is shifted to higher values of ψ'_{nr} and, whereas the Fermi gas cuts off abruptly and is only nonzero within the Fermi

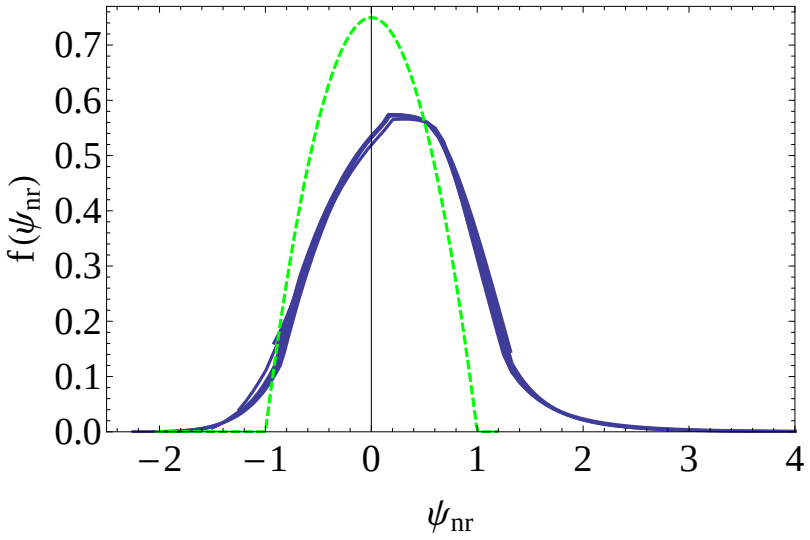

FIG. 11: (color online) The scaling function of our model (blue online) displayed versus the non-relativistic variable ψ_{nr}. The momentum transfer range is the same as in the previous two figures. For reference the Fermi gas result is shown as a dashed curve (green online); clearly, by construction, it scales perfectly.

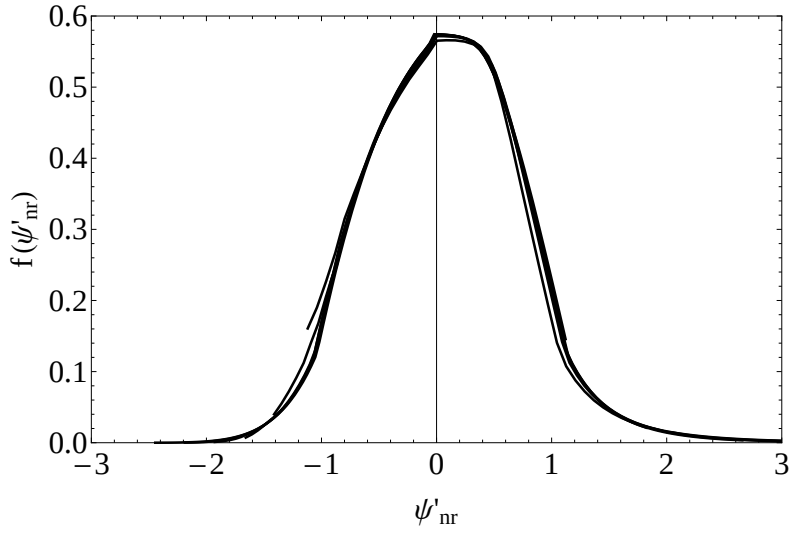

FIG. 12: The scaling function of our model displayed versus the scaling variable of Eq. (38) for the same values of q used in Fig. 11.

cone, the present model produces strength extending to very large and small values of ψ'_{nr}, in accord with experiment. It is worth remarking that if the high momentum tail in the momentum distribution in Eq. (2) is set to zero (*i.e.,* β_1 is set to zero) then these tails extending to large $|\psi'_{nr}|$ essentially disappear. While setting β_1 to zero is not simply setting

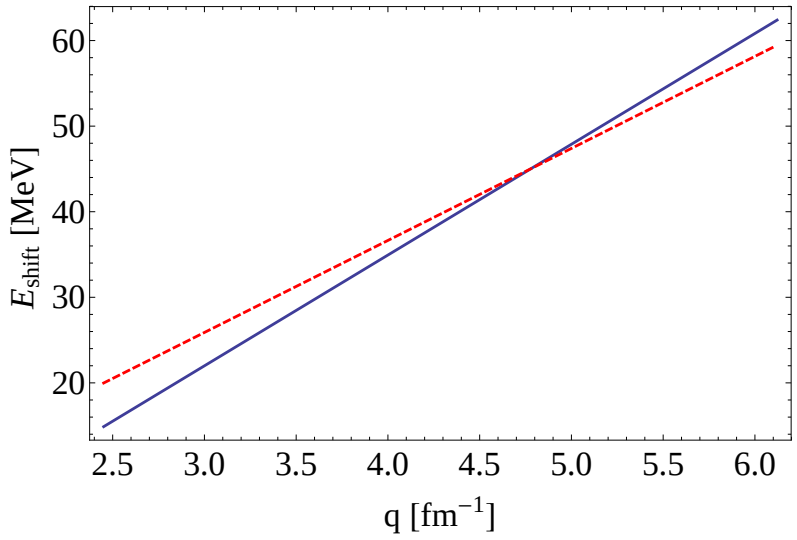

FIG. 13: (color online) The q-dependent energy shift in Eq. (39) (solid curve, blue online) together with the energy shift obtained in RMF studies of ^{12}C (dashed curve, red online).

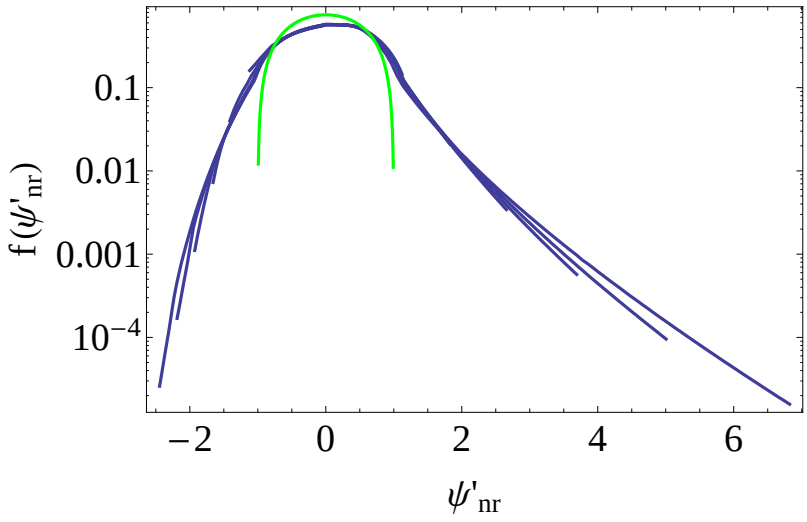

FIG. 14: (color online) As for Fig. 12, but now on a semilog scale.

the part of the momentum distribution arising from short-range correlations to zero, since the long-range correlations also move some strength from below the Fermi surface to somewhat above it, it is very suggestive that in the present model the origin of the tails in the scaling function are principally due to the short-range physics, as is often assumed to be the case. Interestingly, the position of the peak is largely unaffected by "turning off" the high-k part of the momentum distribution, suggesting that the peak position is not strongly correlated with the short-range physics, but rather with the long-range physics.

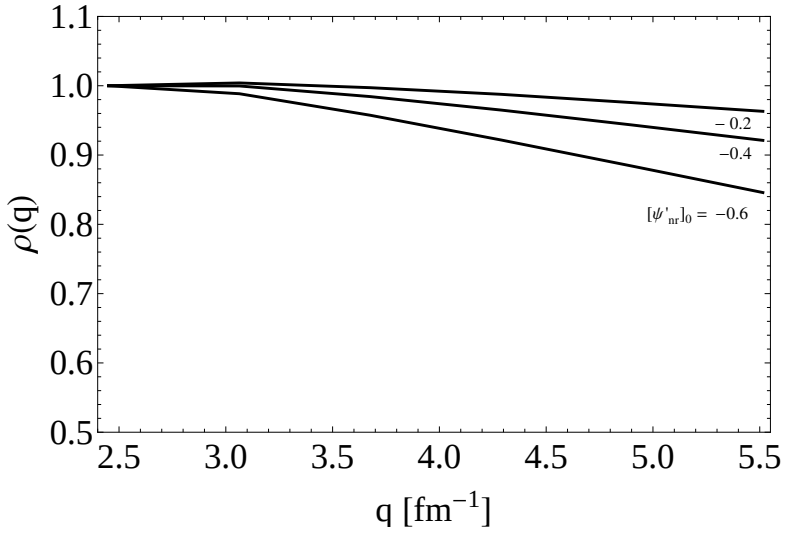

FIG. 15: The scaling function versus q for $[\psi'_{nr}]_0 = -0.6$, -0.4 and -0.2, *i.e.,* in the scaling region.

In concluding this section we address the problem of how the scaling regime is approached. We do so using the scaling variable $[\psi'_{nr}]_0$, where, to make this closer to what has been used in analyses of experimental data [1] a constant energy shift $E_{shift} = 30$ MeV has been chosen in using Eq. (38); this is indicated by the subscript "0". We display f as a function of q for three values of the scaling variable in the scaling region, *i.e.,* to the left of the QE peak. The curves are shown normalized at $q = 2k_F$, namely, the ratio

$$\rho(q) \equiv f(q, [\psi'_{nr}]_0)/f(2k_F, [\psi'_{nr}]_0) \tag{40}$$

is displayed. From Fig. 15 it clearly appears that the scaling regime is approached from above, an occurrence which is qualitatively in accord with experimental findings.

VI. CONCLUSIONS

In the present study we have developed a model centered around an assumed form for the momentum distribution of nucleons in nuclei. The momentum distribution has been chosen to reflect current understanding of how dynamical effects underlying the nuclear many-body problem lead to a form for $n(k)$ with both low-k components coming from long-range interactions and an extended tail at high-k arising from short-range interactions. We have restricted the scope of the study to infinite, homogeneous nuclear matter, have employed only point nucleons, have assumed a strictly non-relativistic model (although in future work

we hope to extend the scope to relativistic modeling), and have restricted our attention to the longitudinal electromagnetic response, for the present.

Working with this as a basis we have developed the formalism in two different directions, maintaining as much consistency as possible. First, we have devised a single-particle Green function that leads to the know saturation properties of nuclear matter and to realistic particle and hole single-particle energy spectra. Second, we have taken the same Green function to obtain the density-density polarization propagator and, through its imaginary part, have obtained the longitudinal electron scattering response function $R(q,\omega)$ and the scaling function $f(q,\omega)$. For the latter we have explored several aspects of scaling and of scaling violations.

We find that scaling is quite well respected, despite the strength of the NN interactions implicit in the problem. There are seen to be some scaling violations, for instance, those observed as shifts of the quasielastic peak positions as functions of q — indeed these are also seen in relativistic mean field theory. The shape of the scaling function is observed to be more spread out than is the Fermi gas scaling function and the former yields a somewhat lower peak height than the latter, both in rough accord with experiment. Where it is large the scaling function in our model is somewhat asymmetric; however, it is not enough so to agree with experiment. When the tails of the scaling function are examined in detail the asymmetry is more apparent and, indeed, the strength at both very large and very small values of the scaling variable is significant, in accord with experiment. If the high-k contributions to the momentum distribution are "turned off" then these tails disappear, suggesting that their origin lies in the part of the momentum distribution arising from short-range correlations. The position of the peak, however, appears to be due to long-range physics.

In summary, the present study has demonstrated that a high level of consistency can be maintained in simultaneously representing both the saturation properties of nuclear matter and the scaling properties of the longitudinal electron scattering response.

Acknowledgments

We thank Dr. Arturo De Pace for valuable help in solving several computational problems. This work is supported in part (T.W.D.) by the U.S. Department of Energy under

cooperative agreement DE-FC02-94ER40818.

---

[1] D. B. Day, J. S. McCarthy, T. W. Donnelly and I. Sick, Ann. Rev. Nucl. Part. Sci. **40**, 357 (1990).

[2] T. W. Donnelly and I. Sick, Phys. Rev. Lett. **82**, 3212 (1999).

[3] T. W. Donnelly and I. Sick, Phys. Rev. C **60**, 065502 (1999).

[4] A. N. Antonov, M. V. Ivanov, M. B. Barbaro, J. A. Caballero and E. Moya de Guerra, Phys. Rev. C **79** (2009) 044602.

[5] J. A. Caballero, J. E. Amaro, M. B. Barbaro, T. W. Donnelly and J. M. Udias, Phys. Lett. B **653**, 366 (2007).

[6] J. E. Amaro, M. B. Barbaro, J. A. Caballero, T. W. Donnelly and A. Molinari, Phys. Rept. **368**, 317 (2002).

[7] A. De Pace, M. Nardi, W. M. Alberico, T. W. Donnelly and A. Molinari, Nucl. Phys. A **726**, 303 (2003).

[8] A. De Pace, M. Nardi, W. M. Alberico, T. W. Donnelly and A. Molinari, Nucl. Phys. A **741**, 249 (2004).

[9] G. Parisi, "Field theory, disorder and simulations", World Scientific (1992), p. 66.

[10] J. E. Amaro, M. B. Barbaro, J. A. Caballero, T. W. Donnelly, C. Maieron and J. M. Udias, Phys. Rev. C **81** (2010) 014606.

[11] J. E. Amaro, C. Maieron, M. B. Barbaro, J. A. Caballero and T. W. Donnelly, Phys. Rev. C **82** (2010) 044601.

[12] M. B. Barbaro, D. Berardo, R. Cenni, T. W. Donnelly and A. Molinari, Phys. Rev. C **80**, 064320 (2009).

[13] K. Gottfried, Ann. of Phys., **21**, 29 (1963).

[14] A. N. Antonov, M. V. Ivanov, J. A. Caballero, M. B. Barbaro, J. M. Udias, E. Moya de Guerra and T. W. Donnelly, Phys. Rev. C **83** (2011) 045504.

[15] W. M. Alberico, R. Cenni, A. Molinari, Rivista del Nuovo Cimento **58**, N.4 (1978).

[16] R. D. Amado, Phys. Rev. **C14**, 1264 (1976).

[17] J. A. Caballero, M. B. Barbaro, A. N. Antonov, M. V. Ivanov and T. W. Donnelly, Phys. Rev. **C81**, 055502 (2010).

[18] A. L. Fetter and J. D. Walecka, "Quantum Theory of Many-Particle Systems", McGraw-Hill (1971) p. 69.

[19] R. Cenni, T. W. Donnelly and A. Molinari, Phys. Rev. C **56**, 276 (1977).

[20] C. H. Johnson, D. J. Horen and C. Mahaux, Phys. Rev. C **36**, 2252 (1987).

[21] W. M. Alberico, A. Molinari, T. W. Donnelly, E. L. Kronenberg and J. W. Van Orden, Phys. Rev. C **38**, 1801 (1988).

[22] J. A. Caballero, Phys. Rev. C **74**, 015502 (2006).

[23] J. E. Amaro, M. B. Barbaro, J. A. Caballero, T. W. Donnelly and J. M. Udias, Phys. Rev. C **75**, 034613 (2007).

[24] Note that a different normalization for the momentum distribution is adopted in Refs. [17, 19].